



Available online at www.sciencedirect.com

ScienceDirect

Proceedings
of the
Combustion
Institute

Proceedings of the Combustion Institute 39 (2023) 5561–5569

www.elsevier.com/locate/proci

Plasma-assisted deflagration to detonation transition in a microchannel with fast-frame imaging and hybrid fs/ps coherent anti-Stokes Raman scattering measurements

Madeline Vorenkamp ^{a,*}, Scott A. Steinmetz ^b, Timothy Y. Chen ^b, Xingqian Mao ^a, Andrey Starikovskiy ^a, Christopher Kliewer ^b, Yiguang Ju ^a

^a Department of Mechanical and Aerospace Engineering, Princeton University, Princeton, NJ 08544, USA
^b Sandia National Laboratories, Livermore, CA 94550, USA

Received 6 January 2022; accepted 9 August 2022 Available online 19 January 2023

Abstract

This study examines kinetic enhancement by nanosecond dielectric barrier discharge (ns-DBD) plasma on fuel-lean, $\Phi = 0.7$, dimethyl ether (DME), oxygen (O₂), and argon (Ar) premixture during deflagration to detonation transition (DDT) experiments in a microchannel. Nonequilibrium plasma produces active species and radicals as well as fast and slow heating of a mixture to promote ignition due to energetic electrons, ions, and electronic and vibrational excitations. Experiments are conducted to examine the influence of the plasma discharge on the premixture and on the resultant deflagration to detonation transition (DDT) onset time and distance through the use of high-speed imaging and one-dimensional, two-beam, femtosecond/picosecond, coherent anti-Stokes Raman scattering (CARS). A high-speed camera is used to trace the time histories of flame front position and velocity and to identify the dynamics and onset of DDT. The results show that plasma discharge can nonlinearly affect the onset time and distance of DDT. It is shown that a small number of plasma discharge pulses prior to ignition result in reduced DDT onset time and distance by 60% and 40%, respectively, when compared to the results without pre-excitation by ns discharges. The results also show that an increase of number of the plasma discharge pulses results in an extended DDT onset time and distance of 224% and 94%, respectively. Time history of the deflagration wave speed of DME and the analysis of ignition timescale under the choking condition of the burned gas of the deflagration wave suggest low temperature ignition may play a role for DME near the isobaric choking condition of the burned gas and the DDT. Plasma-induced low temperature oxidation of the reactive mixture is assessed via the CO2 to O2 ratio as measured through fs/ps CARS during the gas excitation in discharges. CARS measurements also confirm negligible vibrational and rotational heating of the gas by discharge. The present experiments demonstrate

E-mail address: msv@princeton.edu (M. Vorenkamp).

^{*} Corresponding author.

the ability of nonequilibrium plasma to alter the chemistry of DME/O₂/Ar premixtures in order to control DDT for applications in advanced propulsion engines.

© 2023 The Combustion Institute. Published by Elsevier Inc. All rights reserved.

Keywords: Nonequilibrium plasma; Deflagration to detonation transition; Coherent anti-Stokes Raman scattering; Dimethyl ether; Low temperature chemistry

1. Introduction

The dominant form of energy conversion in the United States is still combustion, in 2020 80% of electricity generation was from combustion processes [1]. With the reality of climate change, it is undeniable that combustion processes must become more efficient to help curb carbon emissions. Existing gas turbine engines use a constant pressure Brayton cycle, which limits their thermal efficiency. Advanced power generation using a constant volume cycle, such as a rotary detonation engine (RDE), has the potential to increase efficiency by up to 30% [2]. Unfortunately, instabilities of the detonation wave present a major development challenge which prevents the use of fuel mixtures of lower heating values and large channel width.

Detonation can be achieved through a transitional process when the leading shock wave couples with the combustion wave, causing the flame to evolve from a subsonic deflagration to a supersonic detonation. Establishing control of this process, commonly referred to as DDT (deflagration-to-detonation transition) would make RDEs and other pulse detonation engines more feasible and energy efficient [3]. In part due to this potential, the dynamics of flame front and compression waves during flame acceleration (FA) and DDT under near-limit conditions in small channels have recently received increasing interests [4–15]

Methods of DDT control through kinetic accelerants or energy addition have already begun to be explored. Recent studies at Princeton of the kinetic enhancement of microchannel detonation transition by the addition of ozone to acetylene mixtures, showed dramatic reductions in DDT time (by up to 77.5%) and in onset distance [16]. The DDT limit is also extended from an equivalence ratio of 0.3 to 0.2. The enhancement from ozone in the temperature gradient and concentration gradient can be explained by acceleration of chemical energy release in the flame front. By decreasing ignition delay time using O radical addition from ozone thermal decomposition as well as temperature and concentration gradients, detonation onset is accelerated. The addition of O radicals, stemming from ozone thermal decomposition, accelerates chain branching and the ignition delay time.

However, the mechanism of kinetic enhancement in DDT is still not well understood. Unfortunately, ozone thermally decomposes at temperatures above 450 K, making it difficult to use directly in practical engines with elevated temperatures. Therefore, it is desirable to develop a nonequilibrium plasma discharge to directly initiate and accelerate DDT in-situ. Plasma assisted combustion provides a great opportunity to accelerate ignition to detonation transition and to increase detonation stability.

Another mechanism of DDT enhancement is associated with the Zeldovich hot spot theory and ignition gradient theory [17–19]. Discharge can generate the non-uniform gas excitation with a gradient along the detonation wave propagation direction. This gradient forms the distributed ignition delay in the gas mixture with the ignition phase speed equal to the speed of sound. The phase matching between compression waves and combustion waves accelerates the DDT process.

Over the last two decades, plasma has demonstrated potential to reduce emissions, and to enhance combustion in advanced engines and improve fuel reforming processes [20,21]. Fuel oxidation is carried out through a chain mechanism, and by accelerating this mechanism it is possible to reduce ignition delay time kinetically. This can be done through the dissociation and excitation of molecules and active species production by an electron impact, for example, in a nonequilibrium dielectric barrier discharge [20–22]. Nonequilibrium plasmas have demonstrated the ability to reduce ignition delay and to significantly accelerate cool flame chemistry [22-26]. However, little research has been carried out to understand how plasma assisted low temperature chemistry affects DDT.

2. Experimental methods

In this study we aim to examine the influence of a ns-DBD plasma discharge on a combustible premixture with low temperature chemistry and on the resultant deflagration to detonation transition (DDT) onset time and distance through the use of high-speed imaging and one-dimensional (1-D), two beam, femtosecond/picosecond, coherent anti-Stokes Raman scattering (CARS). The plasma-

induced conversion of the reactive mixture to products yields an important benchmark for the chemical activity of the DBD plasma for comparison to plasma-assisted chemistry models. Employing fs/ps CARS in-situ, we characterize the low temperature fuel oxidation by monitoring the ratio of CO₂ to O₂ as a function of number of ns-DBD pulses. Additionally, the extent of rotational and vibrational heating of the O₂ reactant, which may play a role in kinetic enhancement, is directly monitored through the CARS experiments [27].

For this study, a uniform nanosecond (ns) dielectric barrier discharge (ns-DBD) plasma is applied across a 1 mm tall, 4 mm wide, ~60 cm long combustion channel filled with dimethyl ether/oxygen/argon (DME/O₂/Ar). A high-speed camera imaging the combustion chemiluminescence is used to trace the time histories of flame front position and velocity. The applied ns-DBD plasma is studied with hybrid fs/ps one dimensional coherent anti-Stokes Raman scattering (1D CARS) measurements of rotational and vibrational temperature as well as through the consumption of O₂ and production of CO₂.

A dielectric barrier discharge is formed across the channel between copper electrodes isolated from the discharge gap by a Kapton® film of 0.089 mm thickness. The distance between the electrodes is 1 mm, the width of the electrodes corresponded to the width of the channel (4 mm), and the length of the electrodes is 500 mm. A spark gap is installed at a distance of 50 mm from the edge of the DBD electrodes to initiate a combustion wave in the channel. The channel is filled through a needle feed-through at one end, the opposite side of the channel has a needle feed-through serving as a vent valve. Side windows were made of fused silica to allow optical diagnostics. The assembly is clamped together with fasteners through the frame pieces, nylon insulating tubes shield the fasteners to avoid the electric breakdown.

The channel is mounted on a translation stage on an optical table. A schematic diagram of the experimental setup is shown in Fig. 1c. For operation, the fuel and oxidizer are fed through mass flow controllers with an uncertainty of 1%, and then mixed over a \sim 5 m length of tubing. For filling the test section, the channel is initially pumped down to the single Torr level with an oil-free mechanical vacuum pump, the pump is then isolated and the DME/O₂/Ar premixture is pulled into the channel filling to atmospheric pressure. The final equivalence ratio is Φ =0.7 (30% Ar), with an uncertainty of 2%.

The plasma discharge is generated by a DC high voltage supply and pulser (Eagle Harbor, NSP-120–20-N), and is controlled by a signal generator. While atmospheric DBD plasmas typically demonstrate inhomogeneity and streamer formation, we significantly suppressed this using a short discharge gap where the discharge develops at a significant

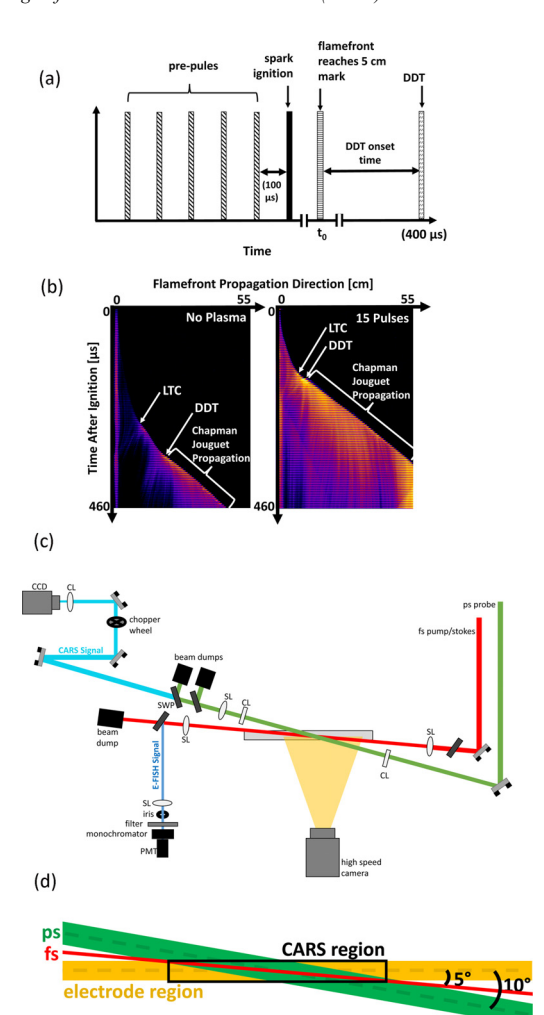


Fig. 1. (a) Timing sequence of the plasma discharge, ignition, and onset of DDT. (b) Stacked fast frame images of flame front progression without (left) and with (right) plasma pre-pulses. Color is added to highlight chemiluminescence intensity. (c) Experimental layout. CL: cylindrical lens, SL: spherical lens, PMT: photomultiplier tube, SWP: short-wave pass filter, CCD: charge couple device camera. (d) Top view close-up highlighting beam crossing angles with electrodes.

overvoltage. The problem of residual nonuniformity is not significant as in this experiment the DBD plasma acts on the entire premixture through which the DDT progresses afterwards, providing significant averaging out of any residual nonuniformity. We estimate the discharge energy from capacitance, C_d , and pulse volage, U, as $W = C_d U^2/2$. A trigger initiates a sequence of 10 kV, 10 kHz, 200 ns pulses ahead of ignition, resulting in an estimated plasma power of 330 W. A variable number of pulses may be applied, with the final pulse 100 μ s prior to spark ignition. The timing is highlighted in Fig. 1(a).

2.1. High-speed imaging

A Phantom v1610 high-speed CMOS camera recording at 200 kHz is used to image the chemiluminescence emitted from the flame-front and trace its propagation position and velocity, as well as to locate the deflagration to detonation transition. The exposure time is 3.69 µs and image resolution is 32 µm resulting in a 8.7 m/s resolution. A UV-NIKKOR, 105 mm, 1:4.5 lens is used without spectral filter. The major emitting/detecting band in these conditions is OH band at 306 nm. A series of false-color images for cases with and without plasma are shown in Fig. 1(b), with important events in the propagation indicated. Once the imaging sequence is complete, the data is processed through MATLAB, and regions of diagnostic interest are identified.

2.2. Hybrid fs/ps coherent anti-Stokes Raman scattering

One-dimensional (1-D), two beam, femtosecond/picosecond, coherent anti-Stokes Raman scattering (fs/ps CARS) technique is employed to probe inside the microchannel. Given the small cell dimensions, the use of fs/ps CARS helps to mitigate the effect of fluorescence and damage in the windows and allows for the direct tracking of rotational/vibrational temperatures and conversion of the reactive mixture to CO₂ through the action of the plasma. Previous work using nanosecond pure-rotational CARS in an open burner demonstrated the ability to simultaneously track concentrations of O2, N2, CO and CO2 in complicated mixtures [28]. The theory and general methods of fs/ps CARS is detailed in [29] and as such, will not be included here. Additional details of the laser system used, and the time-domain modeling of O₂ for simulating the CARS response can be found in [30]. The geometry of the microchannel poses a significant challenge in terms of optical access. The probe region of interest is 1 mm tall, and 4 mm wide with 6 mm thick windows immediately adjacent. Due to the proximity of the windows to the probe region, substantial white light is generated by the fs beam at energies high enough to produce CARS if approaching the cell in a simple orthogonal orientation. This ultimately led to the development and use of an optical configuration similar to that employed in [31] with the exception of using the twobeam phase matching approach [32]. The ps probe is focused to a horizontal sheet with a cylindrical lens of 500 mm focal length, and the fs laser beam is focused to a point using a 700 mm spherical lens which intersects the probe sheet going across it, forming a 1-D region approximately parallel to the length of the microchannel that emits the CARS signal. The ps and fs beams enter the channel at 10° and 5° respectively. The CARS experimental setup is highlight in Fig. 1(c) and 1(d). These shallow incidence angles effectively increase the channel width, placing the focal point at a greater path length from the windows. Despite the fact that a significant percentage of the beam energy is thus reflected at these angles, the probe region receives a higher amount of energy than it would from beams with energy sufficient to avoid white light, at steeper angles. Additionally, due to the significant intensity of reflected beams, the channel is angled in the azimuthal direction to avoid generation of CARS from reflected beams outside of the channel, which would copropagate with the desired signal.

The generated 1D CARS signal is relay imaged to the entrance slit of a 550 mm spectrometer (Horiba iHR550). The signal is separated from the residual probe beam by two angle-tuned shortpass filters (Semrock 561RU). A 600 line/mm grating dispersed the signal onto a CCD (Andor Newton). For the assessment of vibrational heating, the fifth-order diffraction from the grating is used to increase spectral resolution. The first order diffraction resulted in a spectral resolution of 0.70 cm⁻¹ FWHM, while the higher order diffraction yielded a resolution of 0.56 cm⁻¹ FWHM. The small improvement in the slit function allowed for improved resolution of rotational transitions arising from the ground vibrational state and first vibrational state as discussed later.

Once the deflagration regions of interest are identified through the high-speed imaging, the channel is positioned accordingly with the translation stage, relative to the fixed diagnostics. Single-shot 1D CARS images were collected with probe energy of 2 mJ spread over a 1D line of \sim 2 cm and pump/stokes energy of 200 μ J inside the channel.

3. Results and discussion

3.1. High-speed imaging of DDT

For this study, a test case of zero ns-DBD pulses prior to ignition, as well as cases of 10, 15, 20, 30, 50, 100, 200, 500, 1000, 2000, and 5000 prepulses are studied. Two batches (trials of 6) are conducted for the cases with fewer pulses (10-30) and one batch for the higher pulse cases (50–5000). Four batches are conducted for the no-plasma case. These batches are cycled to ensure repeatability. The initial time used in determining the time to onset of DDT is defined as the time at which the flame front has propagated 50 mm such that the onset time is the time required for the flamefront to travel from the 50 mm mark, where X_0 is the edge of the spark electrode nearest the propagation direction, to the point of DDT, and the onset distance is the distance traveled after 50 mm to the point of DDT, this is to ensure the results are independent of variations in initial ignition kernel development [8]. The resultant average onset time and distance are plotted in Fig. 2. It is seen that the cases of 15 to 30

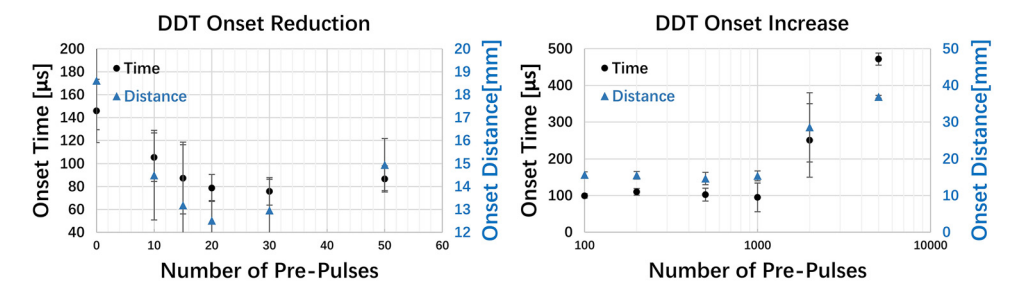


Fig. 2. Average DDT onset reduction (left) and increase (right) in distance and time with error bars for standard deviation.

pre-pulses provide the strongest plasma enhancement of DDT. As will be demonstrated through kinetic simulation and CARS measurements, this is due to the fact that the partial low-temperature fuel oxidation resulting from these plasma pulses is significant enough to kinetically enhance the premixture at the cost of reduction of chemical heat release which will delay DDT in higher pulse counts. Therefore, these kinetic enhancement processes and the heat release reduction process compete with each other in DDT. As a result, at peak, onset distance is reduced from an average of 18.6 cm to 12.5 cm, a 33% reduction. The onset time is reduced from 146 µs to 76 µs, a 48% reduction. In this regime, the kinetic enhancement process dominates. However, with a further increase of pre-pulse numbers (thousands of pulses as compared with tens of pulses) and a significant reduction of heat release rate, we start to see the DDT onset time and distances extended by up to 224% and 94%. In this regime plasma assisted low temperature fuel oxidation dominates the DDT process with the heat release reduction. Therefore, there is an optimum pre-pulse number in plasma assisted DDT. This assessment is supported by the fs/ps CARS data, discussed below, which demonstrates percentage-level plasma induced conversion of reactants to products after thousands of pulses.

To better understand these results, it is helpful to examine the typical velocities of the deflagration fronts over time for the various plasma conditions in Fig. 3. In the control case with no plasma pulses, two distinct velocity peaks occur, one around 70 μ s and one around 115 μ s. This is unique for DME, which has significant low temperature chemistry, and is not observed for C_2H_2 DDT experiments. These are suspected to be caused by the two-stage ignition chemistry of DME. The first stage may be caused due to the presence of low temperature chemistry and the heat loss near the wall, and the second due to the high temperature auto-ignition and DDT where a steep overdriven velocity profile is observed before the front settles down to Chapman-Jouguet velocity. The experimental Chapman-Jouguet velocity is roughly 10% lower than theoretical Chapman-Jouguet velocity due to losses from viscosity and heat transfer. When

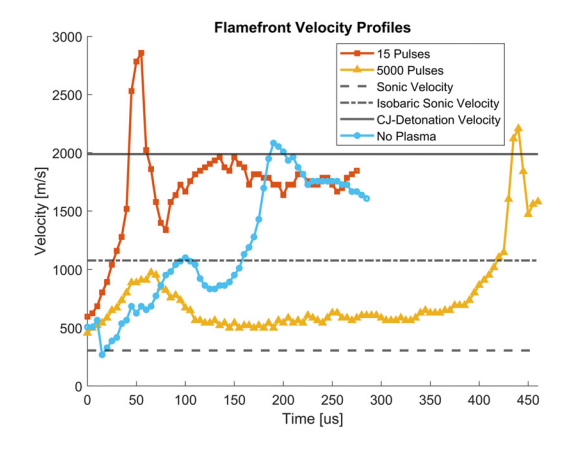


Fig. 3. Characteristic flame-front velocities as a function of time for the control case, no ns-DBD pulses, as well as the cases resulting in the greatest reduction and increase in DDT onset distance and time, 15 pulses and 5000 pulses respectively.

a quantity of 15 DBD pulses is applied, exhibiting the highest degree of DDT enhancement, we see that this gap between stages closes and the high temperature chemistry stage proceeds immediately from the low temperature chemistry stage. The region of negative acceleration is effectively eliminated and there is only one peak in the wave velocity profile before detonation. This is probably due to the plasma assisted ignition chemistry. When 5000 pulses are applied to the mixture prior to ignition, two velocity peaks are once again observed, and the second acceleration event is greatly delayed. This is caused by the over-consumption of the fuel by the pre-ignition ns-DBDs and thus the reduction of the chemical heat release in the deflagration process. This finding underscores the importance of assessing the degree of chemical conversion induced by the plasma pulses, which we elucidate through fs/ps CARS as discussed below. To understand the physics and chemistry of DDT of DME, in Fig. 4, we show an example of a DDT time history without plasma. Here both the flame front's velocity and the two-stage ignition delay time are plotted against the

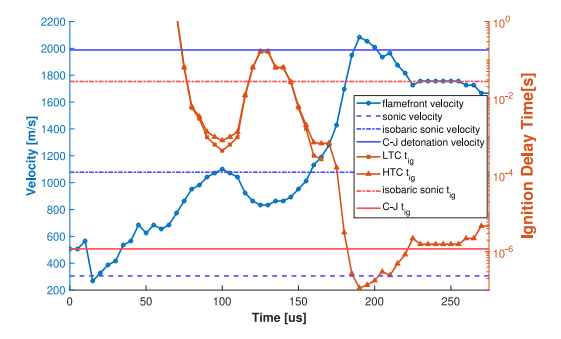


Fig. 4. A typical flamefront velocity profile as a function of time plotted against CHEMKIN simulations of low temperature chemistry (LTC) and high temperature chemistry (HTC) ignition delay time.

time elapsed since the flame reached the 5 cm mark of the microchannel. The ignition delay time is predicted in Fig. 4 [33], as a function of static temperature, T_o , and static pressure, P_o , both of which are calculated from the observed flamefront velocity u_f , where, and,

$$u_u = \left(1 - \frac{\rho_b}{\rho_u}\right) u_f \tag{1}$$

We see that the initial velocity spike appears to peak around the isobaric sonic velocity of the burned gas, before accelerating and settling

$$T_o = T_u + \frac{u_u^2}{2Cp_u} \tag{2}$$

around the C-J velocity at DDT. The match between the first flame front peak velocity and the isobaric sonic speed suggests that the first peak occurs near or at the critical conditions that the burned gas after flame front is choked and enables strong pressure-velocity coupling if there is a sufficient chemical heat release rate at the flame front. Interestingly, near this choking condition, we see the presence of low temperature chemistry in the region, which supports that near the first spike, the low temperature chemistry may affect the DDT processes shown in Fig. 3. It is also seen that near 150 μ s, as the flame front speed increases, there is a low temperature chemistry induced negative temperature coefficient phenomenon. Following this, hot ignition occurs and ignition delay time becomes so short that the burned gas is choked again, leading to a strong ignition and pressure coupling to detonation transition. In addition, it is also seen that after the DDT, the ignition delay time predicted by the measured wave front speed is very close the ignition delay time of the C-J condition. This suggests that the analysis using the ignition delay time at the wave front velocity helps to understand the timescale and chemistry in DDT. Moreover, the experimental C-J velocity is slightly below

the theoretical velocity due to losses like viscosity and heat transfer to the wall.

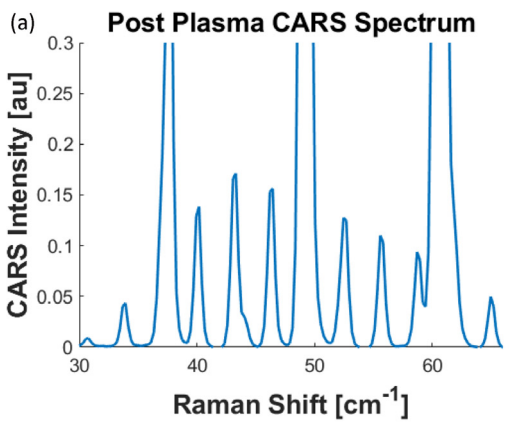
From the analysis in Fig. 4, in the cases with fewer pre-ignition plasma pulses, we see that plasma enhances DDT because of the shortening of the ignition delay time by the active species production in plasma. However, in the cases with a higher number of pulses, although the ignition delay time is reduced, due to the excessive fuel oxidation in plasma discharge, the heat release in the deflagration wave front is reduced which weakens coupling between combustion and the compression wave necessary for DDT. As a result, the DDT is delayed. The nonlinear plasma enhancement of DDT is a direct result of the competition between the kinetic enhancement of ignition and the reduction of heat release rate due to pre-ignition plasma assisted low-temperature fuel oxidation and can ultimately be leveraged to control DDT onset time and position.

3.2. Hybrid fs/ps coherent anti-Stokes Raman scattering

Hybrid CARS is used to evaluate the chemical and thermal effects of the ns-DBD plasma pulses on the combustible mixture. The chemical action is assessed by monitoring the oxidation of the reactants. This is achieved by recording a time-resolved set of CARS spectra for a given number of plasma pulses and evaluating the relative [CO₂]/[O₂] ratio according to the following equation:

$$\frac{[CO_2]}{[O_2]} = \sqrt{\frac{S_{CO_2}}{S_{O_2}}} \times \frac{\sigma_{O_2}}{\sigma_{CO_2}} \times e^{-t\left(\frac{1}{2\tau_{O2}} - \frac{1}{2\tau_{CO_2}}\right)}$$
(3)

where S is the integrated CARS intensity of the particular species, σ is the relevant Raman cross section, t is the probe delay time and τ is the dephasing constant. In the current study, all data were collected at a constant probe delay of 200 ps at near 300 K. Thus, both the ratio of Raman cross sections and dephasing correction terms of Eq. (1) are constant. In this case, calibration experiments in a cell with known pressure ratio of CO₂ and O₂ enable the absolute calibration of the evaluated concentration ratio. As can be seen in Fig. 5(a), the series of ns-DBD plasma pulses clearly results in the production of CO₂. Fig. 5(b) displays the relative CO₂ concentration as a function of DBD pulse number. After several thousand pulses CO₂ is already present in percent-level concentrations relative to O2, with significant global conversion occurring after hundreds-of-thousands of pulses. Notably, this data confirms a chemical effect of plasma pre-pulsing. Unfortunately, only the final product, CO₂, could be monitored here, and concentrations are below detectable levels around the optimal number of pre-pulses (15–30). Several other short-lived intermediaries in the conversion of DME, such as OH, formaldehyde and the previ-



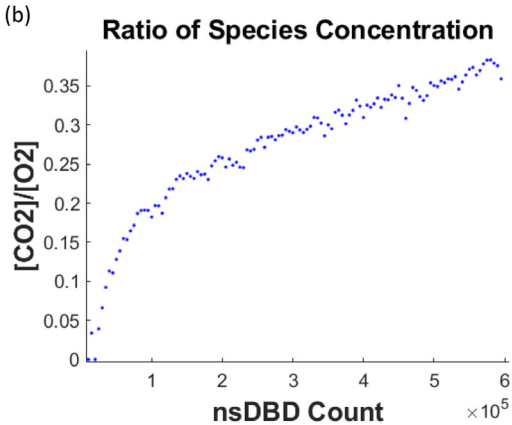


Fig. 5. (a) fs/ps CARS spectra demonstrating the growth of CO2 and depletion of O2 during 1 min of ns-DBD pulses operated at 10 kHz. (b) Calibrated concentration ratio as a function of DBD pulse number in the reactive mixture.

ously discussed O, may be critical in altering DDT onset time. Future measurement of these radicals is necessary to fully understand the chemical effect of the plasma. Nevertheless, the current results demonstrate that small amounts of pre-detonation oxidation are sufficient to impact the detonation wave/heat release coupling, which is in agreement with the overall observation from Fig. 2.

In order to assess the plasma-induced molecular vibrational and/or rotational heating of O₂, the CARS spectra were evaluated for both rotational and vibrational heating 200 nanoseconds after the end of the plasma pulses. Because of rotation-vibration coupling, rotational transitions in vibrationally excited O₂ molecules are slightly red-shifted relative to the rotational transitions of molecules in the ground vibrational state. This shift may be used to evaluate for plasma-induced vibrational nonequilibrium as was recently demonstrated for N₂ in a bare pin-to-pin discharge [27]. In that work, a minimum vibrational heating of

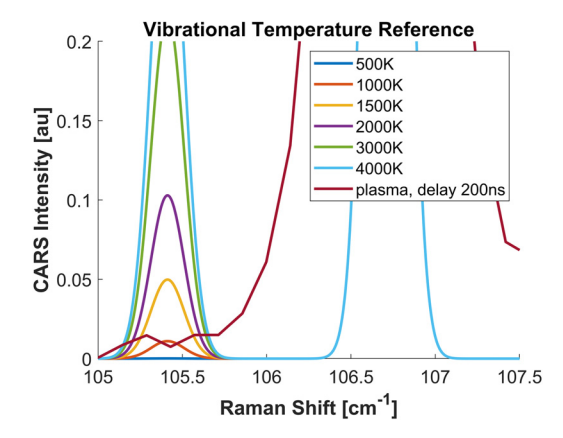


Fig. 6. Pure-rotational fs/ps CARS spectrum of molecular O2 200 ns after a ns-DBD plasma pulse. Only the N"=17 transition is displayed. Simulations of the spectral location and intensity of the rotational transition in v=1 clearly indicate that no observable vibrational heating is induced above 1000 K vibrational temperature. Simulated data assumes no instrument broadening.

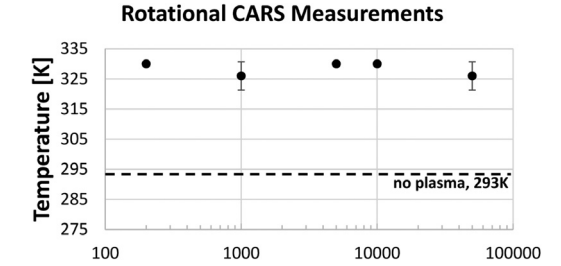


Fig. 7. Averaged rotational temperature measurements of the premixture following 500 plasma pulses at various delay times, error bars show standard deviation. Control case with no plasma included for reference.

Delay [ns]

approximately 1000 K was required to evaluate the population in the first vibrationally excited state. Because of the close spacing of the optical transitions, the 5th order diffraction from the 600 groove/mm grating is used to enhance the spectral resolution of the spectrometer. Fig. 6 shows the measured N" = 17 transition of O_2 , as well as simulated spectra for a range of vibrational temperatures. While the experiment spectrum is broadened by the instrument response, it is clear that no significant vibrational heating of molecular O_2 is induced by the plasma in this system. Furthermore, the evaluated rotational temperatures, shown in Fig. 7 increased by \sim 35 K following 500 plasma discharges, indicating that the ns-DBD plasma is not significantly vibrationally exciting the O_2 molecules. Thus, the decreased DDT onset times observed does not result from vibrational excitation, and more likely is caused by the production of reactive

species by direct electron-impact dissociation that enhance low temperature chemistry.

4. Conclusion

Deflagration to detonation transition experiments in DME/O₂/Ar mixture of atmospheric pressure are carried out. The results show that transversal ns-DBD can chemically sensitize the DME-oxygen mixture and accelerate the DDT transition both in space and time.

The results show that plasma discharge can nonlinearly affect the onset time and distance of DDT. It is shown that a small number of plasma discharge pulses prior to ignition result in reduced DDT onset time and distance while a large number of pre-ignition discharges will delay the DDT. This nonlinear effect is explained by the competition between the plasma enhanced kinetic effect on ignition and the reduced heat release rate in the ignition wave front due to the excessive partial fuel oxidation with many pulses of pre-ignition plasma discharge. For DME mixtures, two distinct flame front peaks were observed. The present experiments and analysis suggest that this unique feature may be caused by the plasma assisted low temperature chemistry of DME.

The present study demonstrates a quantitative effect of the plasma on the premixture temperature and species concentration. In-situ fs/ps CARS measurements evaluated the plasma-induced rate of conversion to CO₂. The results showed that no significant vibrational heating of molecular oxygen is induced. However, the results revealed that plasma assisted low-temperature oxidation increased the CO₂ formation.

The ability to control DDT with plasmas is promising for the development of next generation rocket engines and opens the opportunity to demonstrate further improvement in lean burn flame stability, low temperature fuel oxidation and processing, as well as in emission reduction.

Declaration of Competing Interest

The authors declare that they have no known competing financial interests or personal relationships that could have appeared to influence the work reported in this paper.

Acknowledgements

This work was supported by the DOE grant DE-SC0020233 of Plasma Science Center and the DOE grant DE-SC0021217. MSV was partly supported by the DOE Office of Science Graduate Student Research (SCGSR) Program under the super-

vision of Christopher Kliewer at the Sandia National Laboratory Plasma Research Facility.

CJK: This material is based upon work supported by the U.S. Department of Energy, Office of Science, Office of Fusion Energy Sciences under contract number DE-NA0003525. This research used resources of the Low Temperature Plasma Research Facility at Sandia National Laboratories, which is a collaborative research facility supported by the U.S. Department of Energy, Office of Science, Office of Fusion Energy Sciences. The views expressed in this paper do not necessarily represent the views of the U.S. Department of Energy or the United States Government.

Supplementary materials

Supplementary material associated with this article can be found, in the online version, at doi:10. 1016/j.proci.2022.08.133.

References

- [1] U.S. Energy Information Administration EIA Independent Statistics and Analysis." Electricity in the U.S. U.S. Energy Information Administration (EIA), (www.eia.gov/energyexplained/electricity/electricity-in-the-us.php).
- [2] D. Singleton, S.J. Pendleton, M.A. Gundersen, The role of non-thermal transient plasma for enhanced flame ignition in C2H4-air, J. Phys. D: App. Phys. (4) (2011) 022001.
- [3] National Academies of Sciences, Engineering, and MedicineAdvanced Technologies for Gas Turbines. Thington, DC: The National Academies Press, 2020, doi:10.17226/25630.
- [4] H.-.W. Ssu, M.-.H. Wu, Formation and characteristics of composite reaction shock clusters in narrow channels, Proc. Combust. Inst. 38 (2021) 3473–3480.
- [5] M.-.H. Wu, M.P. Burke, S.F. Son, R.A. Yetter, Flame acceleration and the transition to detonation of stoichiometric ethylene/oxygen in microscale tubes, Proc. Combust. Inst. 31 (2007) 2479-2436.
- [6] M.-.H. Wu, C.-.Y. Wang, Reaction propagation modes in millimeter-scale tubes for ethylene/oxygen mixtures, Proc. Combust. Inst. 33 (2011) 2287–2293.
- [7] M.-.H. Wu, W.-.C. Kuo, Transmission of near-limit detonation wave through a planar sudden expansion in a narrow channel, Combust. Flame 159 (11) (2012) 3414–3422.
- [8] M.-.H. Wu, W.-.C. Kuo, Accelerative expansion and DDT of stoichiometric ethylene/oxygen flame rings in micro-gaps, Proc. Combust. Inst. 34 (2) (2013) 2017–2024.
- [9] E. Dzieminska, A.K. Hayashi, Auto-ignition and DDT driven by shock wave – boundary layer interaction in oxyhydrogen mixture, Int. J. Hydrog. Energy 38 (10) (2013) 4185–4193.
- [10] R.W. Houim, A. Ozgen, S. Oran, The role of spontaneous waves in the deflagration-to-detonation transition in submillimetre channels, Combust. Theor. Model. 20 (6) (2016) 1068–1087.
- [11] W. Han, Y. Gao, C.K. Law, Flame acceleration and deflagration-to-detonation transition in micro- and

- macro-channels: an integrated mechanistic study, Combust. Flame 176 (2017) 285–298.
- [12] H.-.P. Chan, M.-.H. Wu, in: Proceedings of the 26th International Colloquium on the Dynamics of Explosions and Reactive Systems, Boston, USA, 2017 Jul 30th – Aug 4th.
- [13] M.F. Ivanov, A.D. Kiverin, M.A. Liberman, Hydrogen-oxygen flame acceleration and transition to detonation in channels with no-slip walls for a detailed chemical reaction model, Phys. Rev. E 83 (2011) 056313.
- [14] V.N. Gamezo, T. Ogawa, E.S. Oran, Numerical simulations of flame propagation and DDT in obstructed channels filled with hydrogen–air mixture, Proc. Combust. Inst. 31 (2007) 2463–2471.
- [15] T. Machida, M. Asahara, A.K. Hayashi, Three-dimensional simulation of deflagration-to-detonation transition with a detailed chemical reaction model, Combust. Sci. Technol. 186 (2014) 1758–1773.
- [16] J. Sepulveda, A. Rousso, et al., Kinetic enhancement of microchannel detonation transition by ozone addition to acetylene mixtures, AIAA J. (57) (2018) 1–6.
- [17] Y.B. Zeldovich, Regime classification of an exothermic reaction with nonuniform initial conditions, Combust. Flame 39 (2) (1980) 211–214.
- [18] T. Zhang, W. Sun, Y. Ju, Multi-scale modeling of detonation formation with concentration and temperature gradients in n-heptane/air mixtures, Proc. Combust. Inst. 36 (1) (2017) 1539–1547.
- [19] A. Starikovskiy, N. Aleksandrov, Plasma-assisted ignition and combustion, Prog. Energ. Combust. Sci. 39 (1) (2013) 61–110.
- [20] Y. Ju, W. Sun, Plasma assisted combustion: dynamics and chemistry, Prog. Energ. and Combust. Sci. 48 (2015) 21–83.
- [21] N.N. Semenov, "Some problems relating to chain reactions and to the theory of combustion," Dec. 1956, http://nobelprize.org/nobel_prizes/chemistry/ laureates/1956/semenov-lecture.pdf [retrieved 25 Sept. 2008].
- [22] S.M. Starikovskaia, Plasma assisted ignition and combustion, J. Phys. D: Appl. Phys. 39 (2006) R265–R299.
- [23] N.A. Popov, The effect of nonequilibrium excitation on the ignition of hydro- gen—oxygen mixtures, High Temp. 45 (2007) 261–279.

- [24] I.V. Adamovich, I. Choi, N. Jiang, J.-H. Kim, S. Keshav, W.R. Lempert, E. Mintusov, M. Nishihara, M. Samimy, M. Uddi, Plasma assisted ignition and high-speed flow control: non-thermal and thermal effects, Plasma Sources Sci. Technol. 18 (2009) 034018.
- [25] S.M. Starikovskaia, Plasma-assisted ignition and combustion: nanosecond discharges and development of kinetic mechanisms, J. Phys. D: Appl. Phys. 47 (2014) 353001.
- [26] T.Y. Chen, B.M. Goldberg, B.D. Patterson, E. Kolemen, Y. Ju, C.J. Kliewer, 1-D imaging of rotation-vibration non-equilibrium from pure rotational ultrafast coherent anti-Stokes Raman scattering, Opt. Lett. 45 (2020) 4252.
- [27] F. Vestin, P.-.É. Bengtsson, Rotational CARS for simultaneous measurements of temperature and concentrations of N2, O2, CO, and CO2 demonstrated in a CO/air diffusion flame, Proc. Combust. Inst. 32 (2009) 847–854.
- [28] H.U. Stauffer, J.D. Miller, M.N. Slipchenko, T.R. Meyer, B.D. Prince, S. Roy, J.R. Gord, Timeand Frequency-Dependent Model of Time-Resolved Coherent AntiStokes Raman Scattering (CARS) with a Picosecond-Duration Probe Pulse, J. Chem. Phys. 140 (2) (2014) 024316.
- [29] T.L. Courtney, C.J. Kliewer, Rotational coherence beating in molecular oxygen: coupling between electronic spin and nuclear angular momenta, J. Chem. Phys. 149 (2018) 234201, doi:10.1063/1.5058766.
- [30] C.J. Kliewer, High-spatial-resolution one-dimensional rotational coherent anti-Stokes Raman spectroscopy imaging using counterpropagating beams, Opt. Lett. 37 (2011) 229–231.
- [31] A. Bohlin, B.D. Patterson, C.J. Kliewer, Communication: simplified two-beam rotational CARS signal generation demonstrated in 1D, J. Chem. Phys. 138 (2013) 081102.
- [32] H. Zhao, X. Yang, Y. Ju, Kinetic studies of ozone assisted low temperature oxidation of dimethyl ether in a flow reactor using molecular-beam mass spectrometry, Combust. Flame 173 (2016) 187–194.
- [33] X. Yang, X. Shen, J. Santner, H. Zhao, Y. Ju, Princeton HP-Mech. http://engine.princeton.edu/ mechanism/HP-Mech.html, 2017.